J. Synchrotron Rad. (1999). **6**, 293–295

Solving the structure of nanoparticles by multiple-scattering EXAFS analysis

Anatoly I. Frenkel[a*†]

[a]*Materials Research Laboratory, University of Illinois at Urbana-Champaign, Urbana, IL 61801, USA.*
Email:frenkel@bnl.gov

The particle size effect on the coordination number in nanoparticles is much stronger for more distant coordination shells than for the first nearest neighbor shell. We show, using the EXAFS analysis of carbon-supported Pt and Pt-Ru nanoparticles, that it is possible to analyze the structure of mono- and heteroatomic particles through the 4th shell by taking into account multiple scatterings, and by using multiple edge refinement in the case of Pt-Ru alloy. Combined with the transmission electron microscopy and electron diffraction results, our procedure enabled us to obtain the particle shape and size in both types of the nanoclusters, and non-statistical distribution of Pt and Ru atoms in the alloy.

Keywords: nanoparticles, particle size, EXAFS

1. Introduction

Coordination number of nearest neighbors (NN) in nanoparticles is a nonlinear function of the particle diameter if the latter is smaller than 3-5 nm. This property is widely used in EXAFS analysis to determine the size of the nanoparticles. However, the first shell analysis does not provide the coordination numbers and mean square disorder in the 1NN bond lengths unambiguously, due to the correlation between them and other fitting parameters, as well as due to the model dependence of the analysis procedure.

Simple calculations show that the particle size effect on the coordination number is much stronger for the more distant shells. This effect can be demonstrated if one calculates the average coordination numbers for the first few NN shells vs particle size for a given particle shape. In this work, we used hemispherical *fcc* cubeoctahedron as a model of the particle structure, as confirmed by TEM and electron diffraction measurements of supported Pt and Pt-Ru catalysts we investigated [Nashner, 1997, 1998]. The average coordination numbers N_i calculated for this model are shown in Fig. 1. This figure demonstrates that the coordination numbers of the nearest neighbors from 2nd through 4th coordination shells change more rapidly with particle size than the 1NN coordination number.

The results of this and other [Greegor, 1980; Mansour, 1983] model calculations suggest that the reliability of the particle size determination would be increased if coordination numbers were obtained for the higher shells. The entire set of coordination numbers, with their uncertainties, obtained for few first NN shells provides the information about both the shape and the size of the nanoclusters, whereas the information contained in the 1NN coordination numbers only is insufficient to make such a determination [Greegor, 1980].

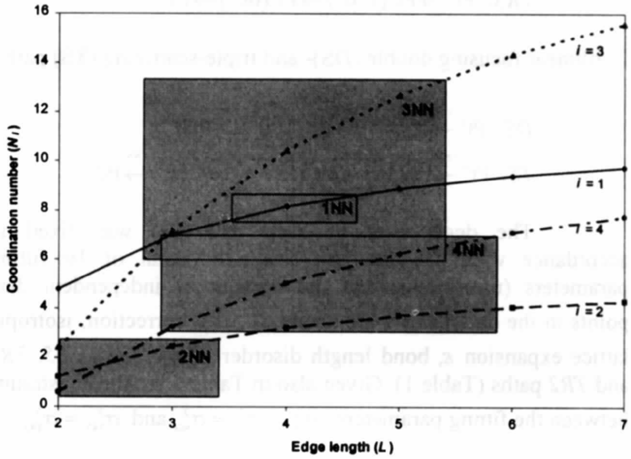

Figure 1
Average coordination numbers N_i of i^{th} ($1 \le i \le 4$) shell in the hemispherical cuboctahedra with different edge length L ($2 \le L \le 7$). Coordination numbers with their uncertainties obtained from the fit to the Pt nanoparticles L_3 edge EXAFS data are shown as shaded rectangles.

2. Multiple-scattering EXAFS analysis of nanoparticles

Our EXAFS study of supported Pt and Pt-Ru nanoclusters shows that it is possible to analyze the structure of mono- and heteroatomic nanoparticles through the 4th NN shell by taking into account multiple scatterings, and by multiple edge refinement (in the case of heteroatomic alloy). To reliably analyze the nanoparticles, our method was first calibrated using the data for the bulk Pt foil where the coordination numbers are known.

2.1 Bulk Pt metal

Pt L_3 edge EXAFS data in Pt foil were measured at 190 K in transmission at the UIUC/Lucent Technologies beamline X16C, National Synchrotron Light Source at Brookhaven National Laboratory. Theoretical $\chi(k)$ was constructed using FEFF6 code [Zabinsky, 1995] and fitted to the data in r space using the FEFFIT code which is part of the UWXAFS data analysis package [Stern, 1995].

The following photoelectron paths were found the most important for the adequate description of the EXAFS data through 6.2 Å, corresponding to the 5th NN in the *fcc* structure with lattice parameter a = 3.92 Å: 5 single – scattering (SS1-SS5) paths from the central (absorbing) Pt^0 atom to its first NN Pt^i ($i = 1,5$); 3 non-collinear scattering paths (scattering angle at the NN site is given in parentheses; symbol above the arrow connecting two adjacent scattering atoms indicates the distance between them):

$$TR1:\ Pt^0 \overset{1NN}{\rightarrow} Pt^1(120°) \overset{1NN}{\rightarrow} Pt^1(120°) \overset{1NN}{\rightarrow} Pt^0;$$

$$TR2:\ Pt^0 \overset{1NN}{\rightarrow} Pt^1(150°) \overset{3NN}{\rightarrow} Pt^1(150°) \overset{1NN}{\rightarrow} Pt^0;$$

[†] Mailing address: Building 510 E, Brookhaven National Laboratory, Upton, NY 11973, USA

$$TR3\text{: } \mathrm{Pt}^0 \xrightarrow{3NN} \mathrm{Pt}^3(150°) \xrightarrow{1NN} \mathrm{Pt}^1(60°) \xrightarrow{1NN} \mathrm{Pt}^0;$$

2 collinear focusing double (DS)- and triple-scattering (TS) paths:

$$DS\text{: } \mathrm{Pt}^0 \xrightarrow{1NN} \mathrm{Pt}^1(0°) \xrightarrow{1NN} \mathrm{Pt}^4(180°) \xrightarrow{4NN} \mathrm{Pt}^0;$$

$$TS\text{: } \mathrm{Pt}^0 \xrightarrow{1NN} \mathrm{Pt}^1(0°) \xrightarrow{1NN} \mathrm{Pt}^4(180°) \xrightarrow{1NN} \mathrm{Pt}^1(0°) \xrightarrow{1NN} \mathrm{Pt}^0;$$

The degeneracy of each path (*N*) was fixed in accordance with the bulk *fcc* structure. Total of 10 fitting parameters (much less than the number of independent data points in the data (36)) were used: S_0^2, ΔE_0 correction, isotropic lattice expansion ε, bond length disorder σ^2 for *SS1* - *SS5*, *TR1* and *TR2* paths (Table 1). Given also in Table 1 are the constraints between the fitting parameters: $\sigma^2_{DS} = \sigma^2_{TS} = \sigma^2_{SS4}$ and $\sigma^2_{TR3} = \sigma^2_{TR2}$.

Fit to the k^2 - weighted $\chi(k)$ in *r*-space is shown in Fig. 2 (a). Excellent agreement was found between the σ^2 obtained for the *SS1* path in the fit (0.0029(3) Å^2) and that predicted by the Einstein model using the known value of the Pt Debye temperature, 225 K. Both this agreement and that between the lattice parameter obtained in the fit (3.914(4) Å) and that assumed in the model (3.92 Å), attest the reliability of our procedure. S_0^2 was obtained to be 0.81(6) and fixed for the subsequent fits to Pt and Pt-Ru nanoclusters.

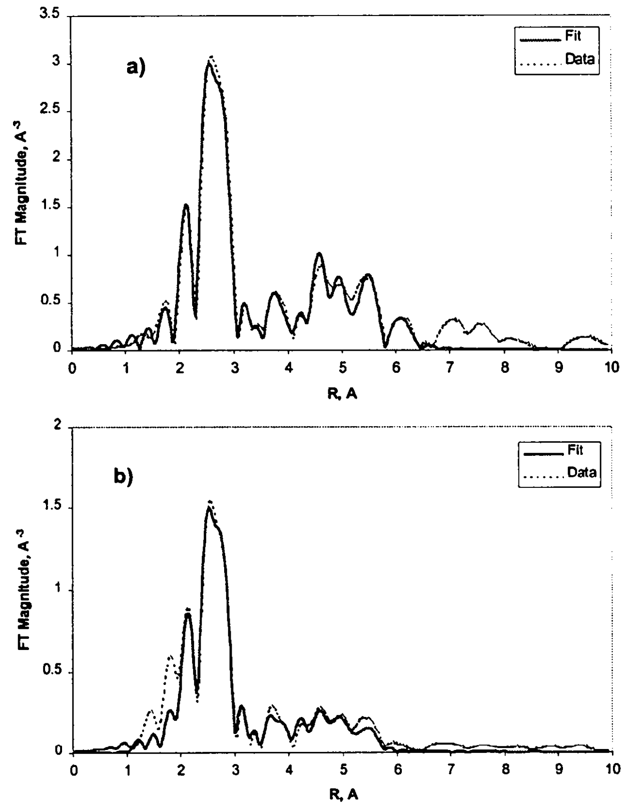

Figure 2
Fourier transform magnitudes of k^2-weighted $\chi(k)$ (data and fit) for the L_3 edge EXAFS in bulk Pt (a) and carbon-supported Pt nanoclusters (b).

2.2 *Carbon-supported Pt nanoparticles*

The procedure tested in the previous subsection for the bulk Pt structural analysis was applied to carbon-supported Pt nanoparticles (E-TEK, Pt L_3 edge EXAFS measured at 190 K) where the structure was found by electron diffraction to have the same *fcc* symmetry as in the bulk. Because of the size effect described in the Introduction, the path degeneracy *N* should be a fitting parameter, in addition to other fitting parameters introduced in the previous subsection. Since the nanoparticles were established with TEM to have hemispherical, i.e., convex structure, the following relationships between the degeneracy of multiple scattering and single scattering paths should hold true (Table 1): $N_{DS} = 2N_{SS4}$; $N_{TS} = N_{SS4}$; $N_{TR2} = N_{TR1}$; $N_{TR3} = 2N_{TR1}$. These constraints, as well as those for the σ^2 described above, were applied during the fits. S_0^2 was fixed as 0.81 as obtained in the fit to the Pt foil EXAFS data. There were 35 independent points in the data and 13 variables in the fit: in addition to σ^2, ΔE_0 and ε, we varied *N* for *SS1* – *SS4* and *TR1* paths (Table 1). Fourier transform magnitudes for the data and fit are shown in Fig. 2 (b). Results are given in Table 1.

Paths	Foil			Nanoparticle		
	N	*R*, Å	σ^2, Å	*N*	*R*, Å	σ^2, Å
SS1	12	2.77	0.0029(3)	8.1(5)	2.75	0.0047(3)
SS2	6	3.91	0.0053(18)	1.6(1.2)	3.89	0.0041(39)
TR1	48	4.15	0.001(5)	10(6)	4.13	0.002(14)
SS3	24	4.79	0.0041(5)	9.7(3.7)	4.77	0.0058(16)
TR2	48	5.16	0.0033(19)	*TR1*	5.14	0.0003(21)
TR3	96	5.16	*TR2*	2×*TR2*	5.14	*TR2*
SS4	12	5.53	0.0059(8)	5(2)	5.51	0.0091(31)
DS	24	5.53	*SS4*	2×*SS4*	5.51	*SS4*
TS	12	5.53	*SS4*	*SS4*	5.51	*SS4*
SS5	24	6.19	0.0081(21)	-	-	-

Table 1
Path parameters varied in the fits to the bulk Pt foil and carbon-supported Pt nanoclusters EXAFS data. *N* is the degeneracy of the path (fixed for the fits to the bulk *fcc* Pt data), *R* is the half path length obtained from the fits assuming isotropic lattice expansion ε.

Using the hemispherical cuboctahedron as a model of the Pt nanoparticles structure, the average coordination numbers, obtained for the shells 1 through 4, were all found to be consistent with the edge length of the cuboctahedron of 3-4 atoms (corresponding to the particle diameter of ~ 15-20 Å). This result agrees with those previously published [Hardeveld, 1989]. Even though the uncertainty in the coordination numbers obtained for the shells 2 to 4 is larger than for the 1st NN shell, the reliability of the size determination is higher since the obtained set of the numbers, within their uncertainties, is consistent with both the size and the shape (hemispherical) of the carbon-supported nanoparticles.

2.3 *Carbon-supported [PtRu$_5$] nanoparticles*

The data analysis procedure outlined above was applied for the analysis of carbon – supported Pt:Ru 1:5 nanoparticles [Nashner, 1997], the *in situ* EXAFS study of their evolution from molecular cluster precursors [Nashner, 1998] and carbon support effect on their size and metallic character [Hills, 1999].

The analysis of the binary alloy nanoparticles is more complicated than that of the pure Pt. Several simplifying approximations used in the previous subsection are no longer valid for the alloy: e.g., there are no constraints between the NN bond lengths, owing to the lack of long range order and random substitution of atoms of different types. That means that the corrections ΔR to the model bond lengths should be varied independently for all paths in the FEFF calculation used in the fits. Therefore, additional constraints are required to reduce the number of variables (the detailed procedure is described in [Nashner, 1997]), e.g.:

1. The most dominant, collinear *DS* and *TS* paths only were included in the theory, in addition to the *SS* paths from *SS1* through *SS4*;
2. σ^2 for Pt-Pt, Pt-Ru and Ru-Ru NN bonds were constrained to be the same for all NN shells, from 1 through 4th. This asumption results in the underestimation of the higher shell coordination numbers because these shells are expected to have larger σ^2 than the first nearest neighbor shells;
3. The ratio of the numbers of interatomic bonding interactions $N_{\text{Pt-Ru}}$ to $N_{\text{Ru-Pt}}$ was fixed in accordance with the 5:1 composition for all shells;
4. FEFF6 paths were fit to both the Pt L_3 and Ru *K* edge EXAFS data simultaneously; the heterometallic bond lengths and σ^2 were constrained to be the same as seen from each central atom.

The local metal coordination environment obtained by the multiple scattering analysis with simultaneous, multiple edge (Pt L_3 and Ru *K*) EXAFS data refinement (Fig. 3) reveals the presence of a nonstatistical distribution of different metal atoms in the nanoparticles [Nashner, 1997]. Specifically, they show a marked preference for segregation of Pt atoms to the particle surface in the fully reduced particles. They were shown to have adopted a hemispherical cuboctahedron *fcc* structure with an average diameter of ~ 15 Å.

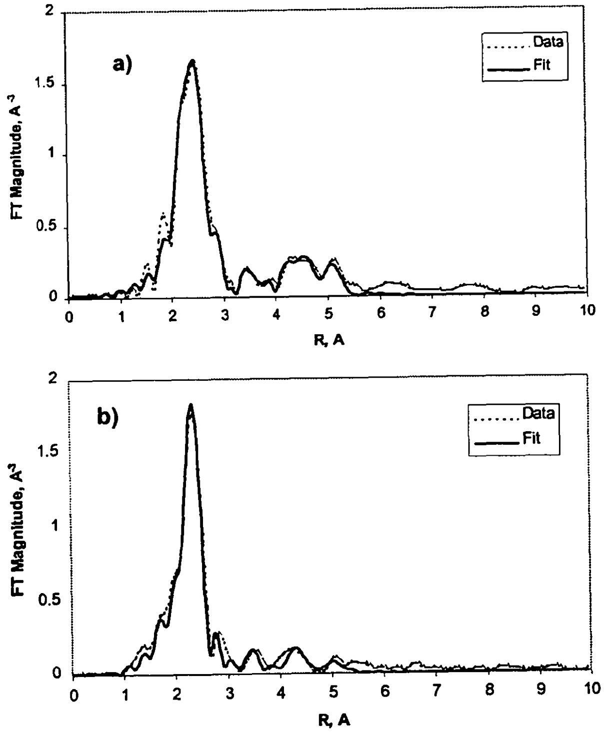

Figure 3
Fourier transform magnitudes of k^2-weighted $\chi(k)$ (data and fit) for the Pt L_3 edge (a) and Ru *K* edge (b) EXAFS in carbon-supported [PtRu$_5$] nanoclusters.

3. Conclusions

We developed a universal EXAFS data analysis procedure which enabled us to model mono- and heteroatomic nanoparticles using the multiple-scattering FEFF6 theory. The procedure was tested using Pt L_3 edge EXAFS data for carbon-supported Pt nanoparticles, and using both Pt L_3 and Ru *K* edge data for Pt-Ru clusters. Coordination numbers and Debye-Waller factors were obtained for all 4 nearest neighbor shells analyzed. Combined with the results of transmission electron microscopy and electron diffraction, this information allowed us to determine the size and shape of the nanoparticles (and their segregation habits for the alloys) with much higher accuracy than using the first shell EXAFS data analysis only.

I would like to thank M. S. Nashner, R. N. Nuzzo and J. R. Shapley for many helpful discussions. This work was supported by the DOE Grant No. DEFG02-96ER45439 through the Materials Research Laboratory at the University of Illinois at Urbana-Champaign.

References

Greegor, R. B. & Lytle, F. W. (1980). J. Catal., **63**, 476.

van Hardeveld, R. & Hartog, F. (1989). Surf. Sci., **15**, 189.

Hills, C. W., Nashner, M. S., Frenkel, A. I., D. A., Shapley, J. R. & Nuzzo, R. N. (1999). Langmuir, in press.

Mansour, A. N. (1983). Ph.D. Thesis, NCSU.

Nashner, M. S., Frenkel, A. I., Adler, D. A., Shapley, J. R. & Nuzzo, R. N. (1997). J. Am. Chem. Soc., **119**, 7760.

Nashner, M. S., Frenkel, A. I., Somerville, D., Hills, C. W., Shapley, J. R. & Nuzzo, R. N. (1998). J. Am. Chem. Soc., **120**, 8093.

Stern, E. A., Newville, M., Ravel, B., Yacoby, Y. & Haskel, D. (1995). Physica B, **208 & 209**, 117.

Zabinsky, S. I., Rehr, J. J., Ankudinov, A., Albers, R. C. & Eller, M. J. (1995). Phys. Rev. B, **52**, 2995.

(Received 10 August 1998; accepted 16 December 1998)